Bubble motion and size variation during thermal migration with phase change

A.K. Nurse*, G. B. McFadden, and S.R. Coriell
National Institute of Standards and Technology
Gaithersburg, MD 20899

December 10, 2012

Abstract

An analysis of the motion of a spherical bubble in a two-phase (fluid-fluid), single component system with a vertical linear temperature gradient is presented. The model for the migration of an immiscible bubble under the effects of buoyancy and thermocapillarity considered by Young, Goldstein and Block is modified to allow for phase change at the bubble surface. We allow the possibility of both translation of the bubble in the vertical direction and the change of bubble radius with time. Depending on the material parameters, the thermocapillary and buoyancy effects that govern the migration of an immiscible bubble can be overwhelmed by the effects of latent heat generation, resulting in a change in the mechanism driving the motion. For a water-steam system conditions are determined for a stationary bubble in which the effects of buoyancy and thermal migration are balanced. The linear stability of the bubble is considered, and conditions are determined that correspond to small-amplitude oscillations of the position and radius of the bubble. A weakly nonlinear analysis of the solution in the vicinity of the unstable solution is performed, and the results are compared with a numerical solution of the nonlinear equations.

1 Introduction

A liquid drop or gas bubble with a temperature-dependent surface energy, $\gamma = \gamma(T)$, tends to migrate spatially in the presence of a thermal gradient [1]. At a fluid-fluid

*Corresponding author. Tel.: + 1-301-975-2725; fax + 1-301-975-3553, *E-mail address:* asha.nurse@nist.gov

interface the gradient of the surface energy along the surface produces a Marangoni force [2] proportional to $d\gamma/dT$ in the tangential stress balance at the interface. For most systems the surface energy tends to decrease with temperature, and in a frame in which a bubble is at rest, the resulting tangential flow along the interface is from the hotter end of the bubble to the cooler end, which tends to lower the total surface energy of the interface. In a frame at rest in the far-field of the fluid, the bubble then moves into the region of higher temperatures. The component of velocity due to such thermocapillary forces can augment or offset that due to other forces such as buoyancy. For example, when heated from below stationary bubbles of an appropriate radius can be observed in a gravitational field [3].

In this paper we present an extension of the original theoretical analysis by Young, Goldstein, and Block [3] who presented an analytical solution for the thermal migration of an immiscible bubble in the limit of slow flow (viscous forces dominating inertial forces) and quasi-static thermal field (conduction dominating convective heat transfer). Young et al. were able to obtain an explicit expression for the bubble velocity as a function of the temperature gradient, gravitational acceleration, and material properties of the system. Their solution is often used to interpret experimental observations of drop or bubble migration in more complicated situations that include effects such as mass diffusion through the interface or a dynamic change in bubble radius. For example, Hardy [4] observed oscillations of both bubble position and radius for an air bubble in silicone oil that is heated from below (see also [5, 6]). Hardy attributed the oscillations to the diffusion of air into or out of the bubble from the surrounding silicone oil as the bubble moves into regions of higher or lower temperature. At the extremes of the motion where the velocity vanishes he observed good agreement with Young et al.'s predicted relation between bubble radius and temperature gradient. In other work, Califano, Mauri, and Shinnar [7] observed drop motion in a two-phase, density-matched, binary fluid in a horizontal temperature gradient. In that case, with a given temperature gradient the motion of α-phase drops surrounded by the β-phase medium were observed to move in

the opposite direction to that of β-phase drops in the α-phase medium. They pointed out that if drop motion was due primarily to thermocapillary forces the drops should move in the same, not opposite, directions since the Marangoni force is in the same direction in both cases. Neither of these phenomena, oscillation of drop radius and position, or reversal of the direction of migration with an interchange of the drop phase, are predicted by the model of Young et al. with an immiscible interface. Both phenomena are predicted by the model of a two-phase, single-component system with a miscible interface that we consider here.

Generally motivated by the observations by Hardy and by Califano et al. we extend the analysis of Young et al. by considering a drop and its surrounding fluid medium to be different thermodynamic phases of the same single-component material such as water and steam. The drop radius and position are both allowed to change in time as flow normal to the interface occurs due to phase change (evaporation or condensation). This is a simplification of both of the above experimental situations, but the model is at the same time rich enough to include both oscillatory behavior of drop radius and additional modes of translation associated with phase-change effects such as latent heat release that can dominate thermocapillary effects. In our work we retain the assumptions of Young et al. regarding slow flow and quasi-static thermal fields, while including the necessary changes to the solution to include the effects of phase change on the drop position and radius. In so doing, we are able to include in our model some familiar effects from the theory of phase transformations such as nucleation and growth [8, 9], drop stability [9, 10], and the thermal migration of liquid inclusions in a solid matrix [11, 12]. The single expression for the drop velocity obtained by Young et al. is replaced in our work by a pair of coupled autonomous ordinary differential equations for the drop position and radius. The steady states of these equations can readily be examined for stationary drops, and the dependence of the radius of such static drops on the processing conditions can be determined. The stability of the drops can also be studied via a linear stability analysis, which reveals the possibility of oscillatory behavior under some conditions.

Limiting cases of the governing equations are shown to include familiar effects from both hydrodynamics and phase transformations. Numerical solutions of the equations are also presented for the case of a water-steam system, whose material properties are well known. We also perform a weakly-nonlinear analysis of the oscillations in the neighborhood of the instability demarcation.

2 Model

We consider the motion of a single spherical bubble or drop in an unbounded fluid medium. We first describe the processing conditions in a laboratory frame, then transfer to a frame that is co-moving with the instantaneous bubble velocity. A schematic diagram is shown in Fig. 1. Our analysis will apply to either a bubble, with density $\rho' < \rho$, or a drop, with density $\rho' > \rho$, where ρ is the density of the surrounding fluid medium.

2.1 The Laboratory Frame

In the laboratory frame, denoted by spatial coordinates $\tilde{x}$, $\tilde{y}$, $\tilde{z}$, and time t, the fluid at infinity is stationary, and in the absence of the bubble there is an applied temperature field $\tilde{T}(\tilde{x}, \tilde{y}, \tilde{z}, t)$ and a hydrostatic pressure field $\tilde{p}(\tilde{x}, \tilde{y}, \tilde{z}, t)$ of the form

$$\tilde{T} = G\tilde{z} + T_\infty, \quad \tilde{p} = -\rho\, g\, \tilde{z} + p_\infty \tag{1}$$

where ρ is the density, assumed constant, the gravitational acceleration g is in the negative $\tilde{z}$ direction, and a positive temperature gradient, $G > 0$, corresponds to the case of a fluid that is heated from above. Here T_∞ and p_∞ are the uniform temperature and pressure that would prevail if $G = 0$ and $g = 0$; alternatively, they are the temperature and pressure at $\tilde{z} = 0$. (In a finite container bounded by differentially-heated vertical plates at $\tilde{z} = \pm H$, say, the model parameters G, T_∞, and p_∞ might be set by the plate temperatures and the mean pressure.) The presence of the bubble disturbs the thermal and pressure fields by terms that decay at infinity. We assume the bubble is centered at

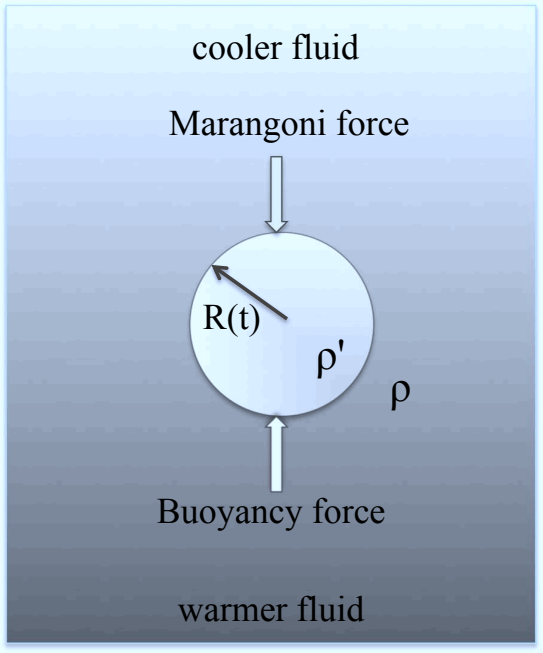

Figure 1: Schematic diagram of a bubble with radius $R(t)$ in a temperature gradient $G < 0$ and gravitational field with acceleration g. The problem is axisymmetric, and in spherical coordinates (r, θ, ϕ) with origin at the bubble center $Z(t)$, the bubble (with density ρ') corresponds to the region $r < R(t)$, and the surrounding fluid (with density ρ) corresponds to $r > R(t)$.

$\tilde{z} = Z(t)$ and moves with a velocity $V = dZ/dt = \dot{Z}$; $V > 0$ then corresponds to a rising bubble.

2.2 The Drop's Frame

In a reference frame (x, y, z) that is co-moving with the instantaneous drop velocity V at a given time t, with coordinates $\tilde{x} = x$, $\tilde{y} = y$, and $\tilde{z} = Z(t) + z$, the fluid at infinity has velocity

$$\mathbf{u} = -V\,\hat{\boldsymbol{z}} + o(1), \tag{2}$$

where $\hat{\boldsymbol{z}}$ is a unit vector in the z direction, and the temperature $T(x,y,z,t) = \tilde{T}(\tilde{x},\tilde{y},\tilde{z},t)$ and pressure $p(x,y,z,t) = \tilde{p}(\tilde{x},\tilde{y},\tilde{z},t)$ have the far-field behavior

$$T = Gz + GZ(t) + T_\infty + o(1), \quad p = -\rho\, g\, z - \rho\, g\, Z(t) + p_\infty + o(1), \tag{3}$$

where $o(1)$ denotes terms that decay at infinity. The drop is then centered at the origin in this frame, and is parametrized by its position $Z(t)$ (in the laboratory frame) and its spherical radius $R(t)$. We employ a spherical coordinate system (r,θ,ϕ) in the moving frame. The solution will be axisymmetric with velocity $\mathbf{u} = u_r(r,\theta)\hat{\boldsymbol{r}} + u_\theta(r,\theta)\hat{\boldsymbol{\theta}}$, where $\hat{\boldsymbol{r}}$ and $\hat{\boldsymbol{\theta}}$ are unit vectors in the r and θ directions. Since we consider a quasi-static model the possible acceleration of the coordinate system does not affect the governing equations.

2.3 The Governing Equations

We assume the flow is governed by the incompressible Stokes equations with a viscosity μ, coupled to a quasi-static thermal field with conductivity k; all material properties (except for the temperature dependence of surface energy) are assumed to be constant. The governing equations outside the drop with $r > R(t)$ are then

$$\nabla p = \mu\nabla^2\mathbf{u} - \rho\, g\, \hat{\boldsymbol{z}}, \quad \nabla\cdot\mathbf{u} = 0, \quad \nabla^2 T = 0, \tag{4}$$

and inside the drop with $r < R(t)$ we have

$$\nabla p' = \mu'\nabla^2\mathbf{u}' - \rho'\, g\, \hat{\boldsymbol{z}}, \quad \nabla\cdot\mathbf{u}' = 0, \quad \nabla^2 T' = 0. \tag{5}$$

Primes will be used to denote dependent variables and material properties inside the drop; neither primes nor subscripts will indicate derivatives.

2.4 The Boundary Conditions

With the notation $\dot{R} = dR/dt$, and with $[\![f]\!] = f - f'$ denoting the jump in the quantity f across the interface at $r = R$, the boundary conditions at $r = R(t)$ are

$$[\![\rho(u_r - \dot{R})]\!] = 0, \quad [\![u_\theta]\!] = 0, \tag{6a,b}$$

$$[\![p - 2\mu\frac{\partial u_r}{\partial r}]\!] = -\frac{2}{R}\left[\gamma_0 + \frac{d\gamma}{dT}(T - T_R)\right], \quad [\![\mu\left(\frac{1}{r}\frac{\partial u_r}{\partial \theta} + \frac{\partial u_\theta}{\partial r} - \frac{u_\theta}{R}\right)]\!] = -\frac{1}{R}\frac{d\gamma}{dT}\frac{dT}{d\theta}, \tag{7a,b}$$

$$[\![T]\!] = 0, \quad [\![k\partial T/\partial r]\!] = L\rho'(u_r' - \dot{R}), \tag{8a,b}$$

$$[\![\frac{1}{\rho}(p - p_R) - s(T - T_R)]\!] = 0. \tag{9}$$

The latter condition is a linearized form of the statement of thermodynamic equilibrium at the interface, $[\![\tilde{g}(T,p)]\!] = 0$, where $\tilde{g}(T,P)$ is the Gibb's free energy density. The equilibrium reference state (T_R, p_R) satisfies $\tilde{g}(T_R,p_R) = \tilde{g}'(T_R,p_R)$. Here $s = -[\partial\tilde{g}(T_R,p_R)/\partial T]$ is the entropy density, and the density is $\rho = [\partial\tilde{g}(T_R,p_R)/\partial p]^{-1}$. The temperature-dependent surface energy has been assumed to have the linearized form $\gamma(T) = \gamma_0 + (T - T_R)d\gamma/dT$, where γ_0 and $d\gamma/dT$ are evaluated at $T = T_R$. Eq. (6a) is the conservation of mass, expressing continuity of the mass flux across the interface; together with Eq. (9) these conditions replace the two kinetic expressions $u_r = 0$ and $u_r' = 0$ that hold at a static immiscible interface as considered by Young et al. Eqs. (7a,b) represent the normal and tangential stress balance at the interface, including capillary effects. Eq. (8b) includes the effect of latent heat release in a change in phase, where the latent heat per unit mass is given by $L = T_R(s - s')$; this term is absent from the balance of heat fluxes in the immiscible case.

In addition we have the far field conditions in Eq. (2) and Eq. (3) and regularity conditions at $r = 0$.

2.5 The Solution

We write the velocity in the form

$$\mathbf{u} = \nabla \times \left[\left(\frac{\psi(r,\theta)}{r\sin\theta}\right)\hat{\boldsymbol{\varphi}}\right] + \nabla\Phi(r,\theta), \tag{10}$$

$$\mathbf{u}' = \nabla \times \left[\left(\frac{\psi'(r,\theta)}{r\sin\theta}\right)\hat{\boldsymbol{\varphi}}\right] + \nabla\Phi'(r,\theta), \tag{11}$$

where ψ and ψ' are Stokes stream functions, Φ and Φ' are velocity potentials and $\hat{\boldsymbol{\varphi}}$ is the unit vector in the ϕ direction. Since the flow is incompressible, Φ and Φ' are harmonic

functions, and in this case will be taken to be radially symmetric, with $\Phi(r) = -b_0/r$ and $\Phi'(r) = 0$. We further write $\psi(r,\theta) = h(r)\sin^2\theta$ and $\psi'(r,\theta) = h'(r)\sin^2\theta$ and find

$$h(r) = \left(\frac{a}{2\mu}\right) r - \frac{V}{2} r^2 + c/r, \quad h'(r) = \left(\frac{a'}{20\mu'}\right) r^4 + b' r^2, \tag{12}$$

where we have imposed regularity at $r = 0$ in the latter, and $u_r \to -V\cos\theta$, or $2h/r^2 \to -V$, in the former. Here a, a', c, and b' are unknowns that are determined by applying the boundary conditions. The corresponding velocity components are given by

$$u_r = \left[\left(\frac{a}{\mu}\right)\frac{1}{r} - V + \frac{2c}{r^3}\right]\cos\theta + \frac{b_0}{r^2}, \quad u_r' = \left[\left(\frac{a'}{10\mu'}\right) r^2 + 2b'\right]\cos\theta, \tag{13}$$

$$u_\theta = -\left[\left(\frac{a}{2\mu}\right)\frac{1}{r} - V - \frac{c}{r^3}\right]\sin\theta, \quad u_\theta' = -\left[\left(\frac{a'}{5\mu'}\right) r^2 + 2b'\right]\sin\theta. \tag{14}$$

The associated pressure fields are harmonic functions that have the form

$$p = -\rho\, g\, r\, \cos\theta - \rho\, g\, Z + \frac{a}{r^2}\cos\theta + p_\infty, \quad p' = -\rho'\, g\, r\, \cos\theta - \rho'\, g\, Z + a'\, r\, \cos\theta + a_0', \tag{15}$$

The temperature fields also admit harmonic solutions given by

$$T = Gr\cos\theta + GZ + T_\infty + \frac{A}{r^2}\cos\theta + \frac{B}{r}, \quad T' = B' r\cos\theta + F'. \tag{16}$$

Here we have also imposed the far field boundary conditions and regularity at $r = 0$. The radially symmetric part of the solution proportional to b_0 in Eq. (13) is due to the net flow normal to the interface that is driven by a density difference upon a change of phase, which appears like a volume source to the far field. Similarly the term proportional to B in Eq. (16) is due to the release of latent heat upon a change of phase, which appears like a heat source to the far field; these effects are both absent in the immiscible model [3].

3 Results

The 12 unknowns, $\dot{R}$, $\dot{Z}$, a, a', a_0', b_0, b', c, A, B, B', and F', are determined by applying the interfacial boundary conditions at $r = R$. The boundary conditions provide 12 linear

inhomogeneous equations in these unknowns; details of which are summarized in the Appendix. If we solve these equations, considering R and Z to be parameters, then the solutions for $\dot{R}$ and $\dot{Z}$ can be regarded as first order ordinary differential equations for $Z(t)$ and $R(t)$. Solving the linear system of equations for $\dot{R}$ and $\dot{Z}$ gives

$$\dot{R} = \frac{g_1(R)Z + g_2(R)}{g_3(R)} \tag{17}$$

$$\dot{Z} = \frac{-GR[e_1(d\gamma/dT) + e_2(s-s')R] + (\rho-\rho')gR^2[e_3(s-s')LR^2 + e_4LR(d\gamma/dT) + e_5]}{d_1LR(d\gamma/dT) + d_2(s-s')LR^2 + d_3}, \tag{18}$$

where $g_1(R)$, $g_2(R)$, and $g_3(R)$ are polynomials in R given by

$$g_1(R) = -k\,\rho\,[2\,G\,d\gamma/dT + G\,R\,\rho'\,(s-s') - g\,R\,(\rho-\rho')], \tag{19}$$

$$g_2(R) = -k\,\{2\rho\gamma(T_\infty) + R\,[(\rho-\rho')(p_\infty - p_R) + (s-s')\rho\rho'(T_\infty - T_R)]\}\,, \tag{20}$$

$$g_3(R) = 4k\,\mu(\rho-\rho') + L\,R\,\rho\,\rho'[2\,d\gamma/dT + R\,\rho'\,(s-s')]. \tag{21}$$

Here the parameters $e_1, .., e_5$, and d_1, d_2 and d_3 depend on the densities, viscosities, and thermal conductivities of the two phases; they are given in the Appendix. We recall that the latent heat and entropy difference are related by $L = T_R(s-s')$; we have retained both in the above equations to help track the origin of the phase change effects: the contributions from L originate from the heat flux equation (8b), and the contributions from $(s-s')$ originate from the interfacial equilibrium equation (9).

The expression for $\dot{R}$ in Eq. (17) is linear in the drop position Z, and provides explicit coupling between the position and radius of the drop. In contrast, Eq. (18) for $\dot{Z}$ is independent of Z. A radius for which the numerator in Eq. (18) vanishes can provide a steady state solution with $\dot{Z} = V = 0$, and a corresponding steady-state value of Z can then be found for this radius by solving Eq. (17) with $\dot{R} = 0$ to give $Z = -g_2(R)/g_1(R)$. The numerator in Eq. (18) has terms proportional to the temperature gradient G and the buoyancy force $(\rho-\rho')g$, which is similar in that respect to the corresponding expression for the drop velocity obtained by Young et al. [see Eq. (22) below]. In our case, however, the coefficients of G and g include contributions from phase change effects, proportional

to the latent heat and entropy difference, that are absent from their model. In addition, their model assumes a constant radius and does not include a governing equation for $\dot{R}$. Our expression for $\dot{R}$ also includes terms in $g_1(R)$ that are proportional to G and g, and the term in $g_2(R)$ includes capillary effects and effects associated with the condition of thermodynamic equilibrium at the interface, which are also absent in the model of Young et al.; their expressions for an immiscible bubble, analogous to Eqs. (17) and (18), are

$$\dot{R} = 0, \quad \dot{Z} = \frac{2}{3\mu(2\mu + 3\mu')} \left[\frac{-\mu}{(2k + k')} 3\, k\, R\, G \frac{d\gamma}{dT} + (\rho - \rho') g\, R^2\, (\mu + \mu') \right]. \tag{22}$$

Since the flow is assumed to be incompressible an immiscible bubble cannot change volume and so $\dot{R} = 0$. The bubble velocity $\dot{Z}$ in Eq. (22) results from a simple balance of the Marangoni and buoyancy forces in the immiscible case, whereas the expression for the velocity of a drop that can change phase in Eq. (18) is considerably more complicated.

In the limit of large latent heat $L = T_R(s - s')$ no phase change occurs and the interface becomes a material surface with no relative mass flux normal to the drop surface. In this limit, or equivalently in the limit of large R, we obtain the velocity

$$V = \left[\frac{e_3}{d_2} \right] (\rho - \rho')\, g R^2 = \left[\frac{2\,(\mu + \mu')}{3\,\mu(2\mu + 3\mu')} \right] (\rho - \rho')\, g R^2, \tag{23}$$

which represents the balance between the forces of gravity and friction due to Hadamard and Rybczynski for an immiscible liquid drop (see Batchelor [13], p. 236). If $\mu' \gg \mu$, this further reduces to Stokes' law for the settling of a solid particle,

$$V = \left[\frac{2}{9\mu} \right] (\rho - \rho')\, g R^2. \tag{24}$$

In Fig. 2 we plot the velocity given by Eq. (18) as a function of the bubble radius for property values corresponding to a water-steam system at $T_R = 373.15$ K as given in Table I. Curves for four values of the temperature gradient G are shown. For a bubble of steam in water, the buoyancy force is in the upward direction, and for $G > 0$ the bubble rises for all values of R. For negative values of G thermal effects tend to oppose those of gravity, and small bubbles fall with a negative velocity. For each value of $G < 0$ there is a radius, whose size depends on G, for which the bubble is stationary; larger bubbles rise

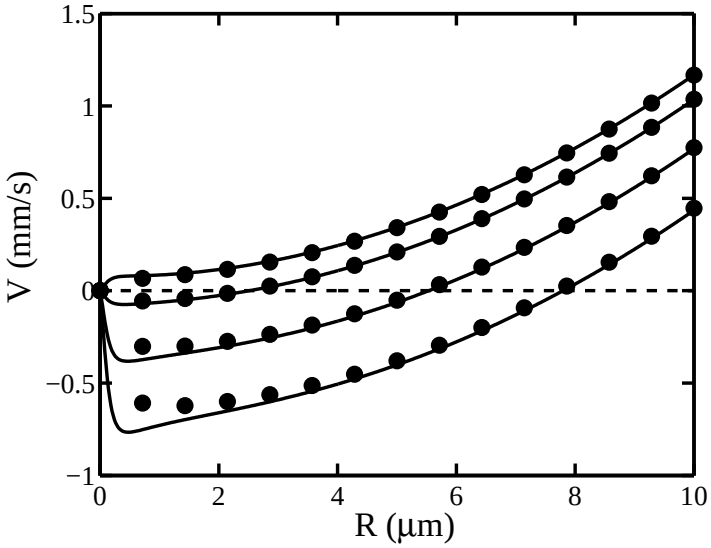

Figure 2: The solid curves show the velocity V as a function of radius R for a bubble of steam in water at $T_R = 373.15$ K for temperature gradients of, from top to bottom, $G = 1000$ K/m, $G = -1000$ K/m, $G = -5000$ K/m, and $G = -10000$ K/m, as given by Eq. (18). The filled circles denote corresponding velocities under the assumption $d\gamma/dT = 0$.

as buoyancy dominates thermal effects. The symbols in the plot indicate the velocities produced if $d\gamma/dT = 0$ is assumed in Eq. (18). These results for $d\gamma/dT = 0$ disagree with the solid curves at small R, indicating that the Marangoni effect is significant in this regime. The results for $d\gamma/dT = 0$ are in good agreement with the solid curves at large radii. Note that in the model of Young et al. setting $d\gamma/dT = 0$ in Eq. (22) eliminates the dependence of the bubble velocity on the temperature gradient G; the variation in the curves in Fig. 2 with G at large R is a phase-change effect, as will be explored in more detail below.

3.1 Steady States

The steady states of Eq. (17) and Eq. (18) correspond to setting $\dot{R} = 0$ and $\dot{Z} = 0$. Solving Eq. (18) for $\dot{Z} = 0$ then gives a relation between G and R,

$$G = \frac{(\rho - \rho')\, g[e_3(s - s')LR^3 + e_4\, LR^2(d\gamma/dT) + e_5 R]}{[e_1(d\gamma/dT) + e_2(s - s')R]}, \tag{25}$$

and then solving Eq. (17) for $\dot{R} = 0$ gives an expression for Z,

$$Z = -\frac{\{2\rho\gamma(T_\infty) + R\,[(\rho - \rho')\,(p_\infty - p_R) + (s - s')\rho\rho'(T_\infty - T_R)]\}}{\rho\,[2\,G\,d\gamma/dT + G\,R\,\rho'\,(s - s') - g\,R\,(\rho - \rho')]}. \tag{26}$$

The large R limit of Eq. (25) is

$$G = \frac{e_3}{e_2}\,(\rho - \rho')\, g\, LR^2. \tag{27}$$

Note that this result is independent of $d\gamma/dT$, but is instead proportional to the latent heat L and to R^2.

The small R limit of Eq. (25) (for $d\gamma/dT \neq 0$) is

$$G = \frac{e_5\,(\rho - \rho')\, g\, R}{e_1(d\gamma/dT)}. \tag{28}$$

The effects of latent heat are unimportant in this limit. This result is similar in form to the immiscible result of Young et al. for stationary drops,

$$G = \frac{(\rho - \rho')\, g\, R\,(2 + k'/k)(1 + \mu'/\mu)}{3\, d\gamma/dT}, \tag{29}$$

which was used by Hardy [4] to analyze the motion of a bubble of air in silicone oil. With the approximation $k' \ll k$, $\rho' \ll \rho$, and $\mu' \ll \mu$, this equation reduces to

$$G = \frac{2\,\rho\, g\, R}{3\, d\gamma/dT}, \tag{30}$$

which agrees with the result in Eq. (28) if the expressions for e_5 and e_1 are evaluated in this limit as well.

If the Marangoni term in the denominator of Eq. (25) is negligible ($d\gamma/dT \approx 0$), then the small R limit takes the form

$$G = \frac{e_5\,(\rho - \rho')\, g}{e_2(s - s')}, \tag{31}$$

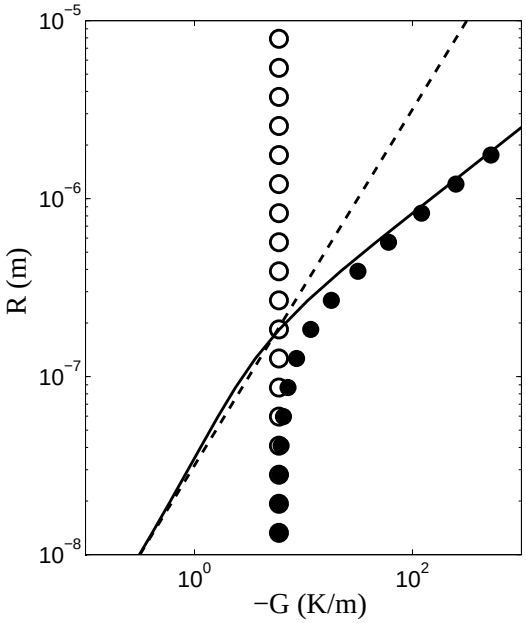

Figure 3: The steady-state radius R versus temperature gradient G for which the velocity V vanishes for a bubble of steam in water that is heated from below at $T_R = 373.15$ K. The solid curve shows the exact relation given by Eq. (25). The dashed curve shows the corresponding results for an immiscible bubble as described by Young, Goldstein, and Block. The filled circles show results obtained by setting $d\gamma/dT = 0$ in Eq. (25). The open circles show results obtained using the small R limit in Eq. (31).

which is independent of R; the entropy difference $(s - s')$ is significant in this limit.

To illustrate these results we consider property values for a water-steam system at $T_R = 373.15$ K and at $T_R = 640$ K (near the critical point, $T_c = 647.096$ K) as given in Table I. For the lower temperature, corresponding to the boiling point at one atmosphere of pressure, the large difference in density between water and steam leads to pronounced buoyancy effects, whereas at the higher temperature the ratios of the densities and other material properties of the two phases approach unity, and the surface energy decreases, which tend to diminish the effects of buoyancy and capillarity.

In Fig. 3 we show steady-state values of R versus G for the case of a stationary bubble of steam in water at $T_R = 373.15$ K that is heated from below ($G < 0$). The solid

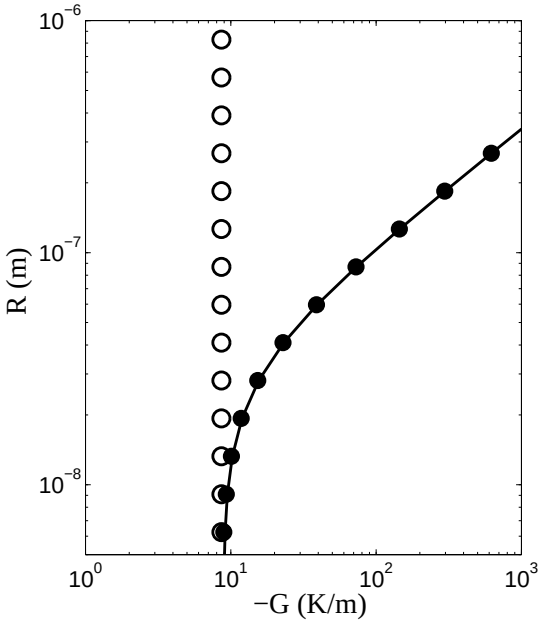

Figure 4: The steady-state radius R versus temperature gradient G for which the velocity V vanishes for a drop of water in steam that is heated from below at $T_R = 373.15$ K. The solid curve shows the exact relation, the filled circles show results obtained by setting $d\gamma/dT = 0$, and the open circles show results obtained using Eq. (31).

curve corresponds to the results given by Eq. (25). For large R the curve asymptotes to the values given by Eq. (27), and for small R the curve asymptotes to values given by Eq. (28). The dashed curve corresponds to the immiscible result of Young et al., and agrees with the solution for small R, indicating a balance between Marangoni and buoyancy forces. The solid and dashed curves differ significantly for large R, where the buoyancy force is instead balanced by thermal effects related to the release of latent heat, as will be discussed in more detail below. The filled circles denote the results obtained by setting $d\gamma/dT = 0$ in Eq. (25), emphasizing that the large R results are insensitive to the Marangoni effect; however these effects cannot be neglected for small R. The open circles denote the small R results in Eq. (31) which also correspond to setting $d\gamma/dT = 0$.

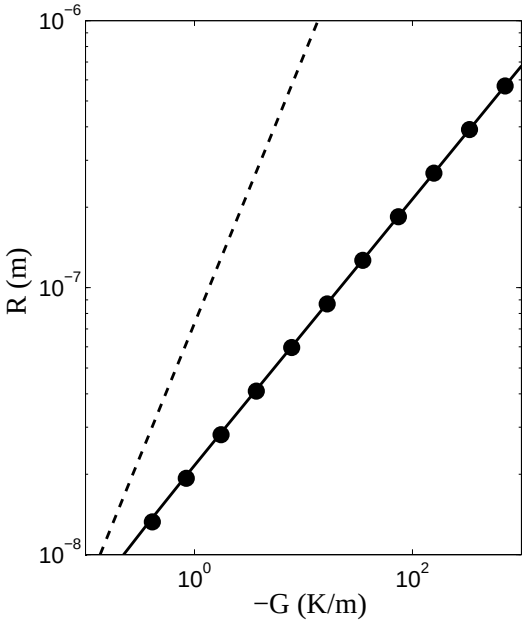

Figure 5: The steady-state radius R versus temperature gradient G for which the velocity V vanishes for a bubble of steam in water that is heated from below at $T_R = 640$ K. The solid curve shows the exact relation, the dashed curve shows the corresponding results for an immiscible bubble as described by Young, Goldstein, and Block, and the filled circles show results obtained by setting $d\gamma/dT = 0$.

Fig. 4 also corresponds to the case of heating from below at $T_R = 373.15$ K, but here we consider instead the case of a stationary drop of water in steam. By inverting the water and steam phases compared to the previous case in Fig. 3, the buoyancy force, proportional to $(\rho - \rho')$, is then downward rather than upward, whereas the Marangoni force remains in the downward direction and cannot balance the force of buoyancy. However, the latent heat L also changes sign under this inversion of phase, so that the balance given in Eq. (27) is still possible. For large values of R the solid curve in Fig. 4 accordingly asymptotes to the relation given in Eq. (27). For small values of R the curve tends to a constant value of G as given by Eq. (31) (open circles). The filled circles, corresponding to $d\gamma/dT = 0$ in Eq. (25), show that the results are insensitive to the Marangoni effect

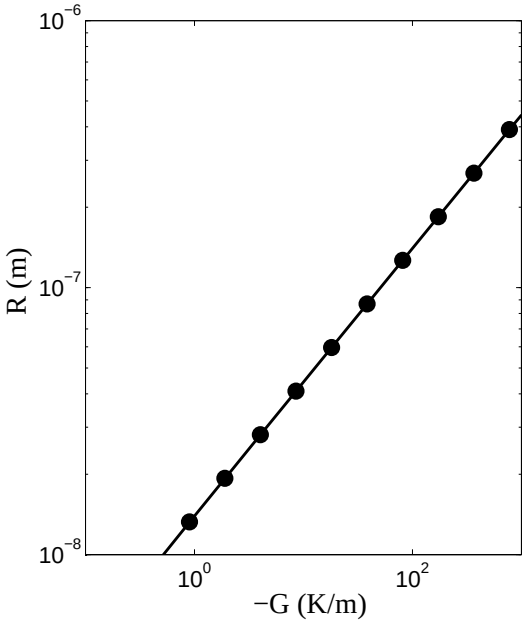

Figure 6: The steady-state radius R versus temperature gradient G for which the velocity V vanishes for a drop of water in steam that is heated from below at $T_R = 640$ K. The solid curve shows the exact relation, and the filled circles show results obtained by setting $d\gamma/dT = 0$.

over the full range of R shown in this case.

In Figs. 5 and 6 we show analogous results at the higher temperature in Table I, $T_R = 640$. In this case the transition to small R behavior occurs at unphysically small radii, and the results shown for $R \geq 10^{-8}$ m all correspond to the large R limit.

In Fig. 7(a) we show streamlines of the flow for a stationary bubble that can change phase. More specifically, the streamlines correspond to contours of the functions $\rho\psi(r,\theta)$ and $\rho'\psi'(r,\theta)$, which are continuous across the phase boundary. The flow penetrates the interface with $u_r \neq 0$ and $u'_r \neq 0$. Because of the density difference between the phases there is a jump in normal velocity across the interface, producing a discontinuity in the slope of the streamlines at the interface while preserving $[\![\rho u_r]\!] = 0$ and $[\![u_\theta]\!] = 0$. The corresponding thermal field is shown in Fig. 7(b). The temperature contours surround the bubble, while the bubble itself is essentially isothermal due to the equilibrium boundary

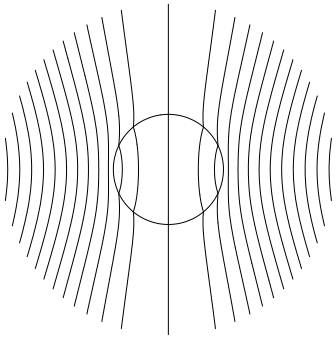

(a) Streamlines of the flow near a stationary bubble that can change phase.

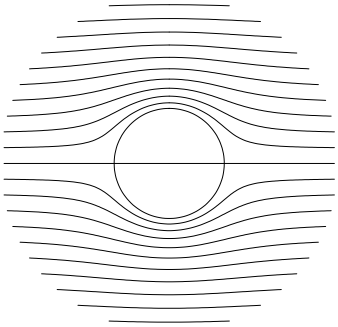

(b) Contours of the temperature field near a stationary bubble that can change phase.

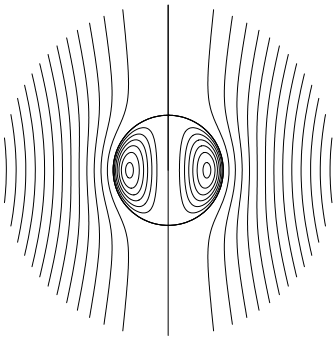

(c) Streamlines of the flow near a stationary immiscible bubble.

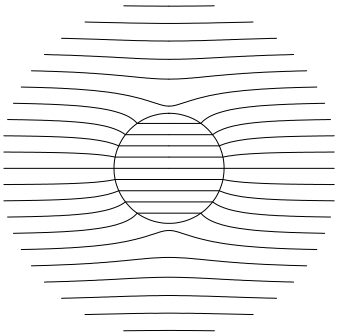

(d) Contours of the temperature field near a stationary immiscible bubble.

Figure 7: Comparison of a drop that can change phase [subfigures (a) through (b)] and an immiscible drop [subfigures (c) through (d)].

condition given in Eq. (9).

The analogous results for a stationary immiscible bubble are shown in Figs. 7(c) and 7(d). In that case the interface is a streamline of the flow, and the interface is a material surface. The thermal field penetrates the bubble, with a discontinuity of slope in the isotherms at the interface due to the difference in thermal conductivities. With equal thermal conductivities the bubble would be transparent to the thermal field, and the temperature contours would be horizontal. These results highlight the qualitative similarities and differences between the cases of immiscible drops and drops that can

change phase.

3.2 Critical Radius

If we set $G = 0$ and $g = 0$ in Eq. (18) the drop is stationary as $V = 0$. From Eq. (17) the radius is also constant, $R = R_N$, if

$$\frac{2\gamma(T_\infty)}{R_N} = \left(1 - \frac{\rho'}{\rho}\right)[p_R - p_\infty] + \rho'\,(s - s')[T_R - T_\infty]. \tag{32}$$

For an isothermal drop with $T = T_\infty$, $\gamma = \gamma(T_\infty)$, and $p_\infty = p_R$ this gives the Gibbs-Thomson relation [9]

$$T_\infty = T_\mathrm{R} - \frac{T_\mathrm{R}\,\gamma}{[\rho'\,L]}\left(\frac{2}{R_N}\right) \tag{33}$$

between the critical drop radius R_N and the system temperature T_∞. More generally, given a uniform temperature T_∞ and pressure p_∞ in the surrounding liquid, from Eq. (9) the equilibrium pressure p' inside the drop satisfies

$$p' = p_R + \frac{\rho'}{\rho}[p_\infty - p_R] - \rho'\,(s - s')\,[T_\infty - T_R], \tag{34}$$

so that Eq. (32) reduces to the Laplace-Young equation for a spherical drop (see Batchelor [13], p. 64)

$$p' - p_\infty = \frac{2\gamma}{R_N}. \tag{35}$$

In the theory of phase transformations an isothermal critical nucleus is normally dynamically unstable. Below we will consider the stability of stationary drops in a temperature gradient and find that, depending on the conditions, they can be either stable or unstable, and the instabilities can be oscillatory in time.

3.3 Relation to Liquid Zone Migration

The results of Eq. (17) and Eq. (18) are also related to a materials processing technique studied by Tiller [11] in which a liquid zone migrates through a solid in a temperature gradient. This mechanism also occurs as a limiting case for a fluid-fluid two-phase system,

as can be illustrated by taking $\rho' = \rho$, $\mu' = \mu$, and $d\gamma/dT = 0$ in (17) and (18). These simplifications produce an isothermal drop that satisfies the Laplace-Young equation. In addition the fluid flow vanishes in the laboratory frame, and the only flow in the reference frame of the drop is a uniform translation of the sample. Under these circumstances Eq. (17) and Eq. (18) reduce to

$$\dot{R} = \frac{-k}{\rho L R}\left[GZ + T_\infty - T_R - \frac{2T_R\gamma(T_\infty)}{\rho L R}\right], \tag{36}$$

$$\dot{Z} = \frac{-G\,e_2}{d_2\,L} = \frac{-3\,k\,G}{\rho\,L}. \tag{37}$$

These relations can also be obtained directly from a simplified phase-change model consisting of the steady state diffusion equation for $T(r,\theta)$ with the assumed far field and interfacial boundary conditions, including the term $u_r = V\cos\theta$ in Eq. (8b). Eq. (37) for $\dot{Z}$ indicates that the drop tends to move with a speed proportional to the temperature gradient and in a direction determined by the sign of the latent heat: inverting the phases for a given temperature gradient reverses the direction of the motion. The driving force for motion in this case is not a mechanical force balance, but represents the rate at which latent heat released at the phase boundary can diffuse into the surrounding liquid while maintaining the interface at equilibrium conditions. In particular, a bubble ($L < 0$) which is heated from below ($G < 0$) tends to sink ($\dot{Z} < 0$) due to the phase-change effect. We also note that the coefficient of Z in Eq. (36), $-kG/\rho' LR$, represents the tendency of the bubble to grow or shrink as the position of the bubble varies relative to the temperature gradient. For example, a bubble sinking ($\Delta Z < 0$) into a hotter region of fluid ($G < 0$) will tend to expand ($\dot{R} > 0$) due to evaporation at the bubble interface.

These mechanisms remain in effect under more general conditions with unequal materials properties, and augments the other processes such as thermocapillarity that also contribute to the bubble motion in Eq. (18).

3.4 Stability of the Steady State

The dynamical equations (17) and (18) can be written in the form

$$\dot{R} = \frac{g_1(R)Z + g_2(R)}{g_3(R)} \tag{38}$$

$$\dot{Z} = \frac{h_1(R)}{h_2(R)}, \tag{39}$$

where the polynomials $g_1(R)$, $g_2(R)$, and $g_3(R)$ are given in Eqs. (19)–(21), and

$$h_1(R) = -GR[e_1(d\gamma/dT) + e_2(s-s')R] + (\rho-\rho')gR^2[e_3(s-s')LR^2 + e_4LR(d\gamma/dT) + e_5] \tag{40}$$

$$h_2(R) = d_1LR(d\gamma/dT) + d_2(s-s')LR^2 + d_3. \tag{41}$$

A steady state $(\bar{R}, \bar{Z})$ is then given by

$$h_1(\bar{R}) = 0, \quad \bar{Z} = -g_2(\bar{R})/g_1(\bar{R}). \tag{42}$$

Writing

$$R(t) \approx \bar{R} + \delta R(t), \quad Z(t) \approx \bar{Z} + \delta Z(t), \tag{43}$$

the perturbations satisfy the linearized equations

$$\frac{d}{dt}\begin{bmatrix} \delta R \\ \delta Z \end{bmatrix} = \begin{pmatrix} \alpha & \beta \\ \epsilon & 0 \end{pmatrix} \begin{bmatrix} \delta R \\ \delta Z \end{bmatrix} \tag{44}$$

where

$$\alpha = \frac{\bar{Z}dg_1(\bar{R})/dR + dg_2(\bar{R})/dR}{g_3(\bar{R})}, \quad \beta = \frac{g_1(\bar{R})}{g_3(\bar{R})}, \quad \epsilon = \frac{dh_1(\bar{R})/dR}{h_2(\bar{R})}. \tag{45}$$

A normal mode solution has the form

$$\begin{bmatrix} \delta R(t) \\ \delta Z(t) \end{bmatrix} = \begin{bmatrix} \delta R(0) \\ \delta Z(0) \end{bmatrix} \exp(\sigma t), \tag{46}$$

where the two eigenvalues $\sigma = \sigma_\pm$ are given by

$$\sigma_\pm = \frac{\alpha \pm \sqrt{\alpha^2 + 4\beta\epsilon}}{2}. \tag{47}$$

The stability of a drop corresponding to a critical nucleus with $\bar{R} = R_N$ as considered in Section 3.2 is obtained for the special case $G = 0$ and $g = 0$. We then have $\beta = \epsilon = 0$, and there is a single mode with $\sigma = \alpha$ given by

$$\sigma = \frac{2k\rho\gamma(T_\infty)}{R_N\,[4k\,\mu(\rho-\rho') + L\,R_N\,\rho\,\rho'[2\,d\gamma/dT + R_N\,\rho'\,(s-s')]]}. \tag{48}$$

If $\rho = \rho'$ and $d\gamma/dT = 0$ this reproduces the classical instability of the critical nucleus with $\sigma = 2kT_R\gamma(T_\infty)/([\rho L]^2 R_N^3) > 0$. If $\rho \neq \rho'$ there is fluid flow normal to the interface that tends to modify the heat transfer from the bubble and affect stability, as reflected by the term proportional to μ in Eq. (48). The term proportional to $d\gamma/dT$ in Eq. (48) can be either stabilizing or destabilizing depending on the sign of the latent heat.

Returning to the general case, depending on the sign of the discriminant in Eq. (47) the growth rates σ are either a pair of real roots or a complex conjugate pair $\sigma_\pm = \sigma_r \pm i\sigma_i$. For neutral stability we require $\sigma_r = 0$. An oscillatory mode with $\sigma_r = 0$ and $\sigma_i \neq 0$ occurs if $\alpha = 0$ and $\beta\epsilon < 0$. From Eq. (45) we find that $\alpha = 0$ if

$$G\,(\rho-\rho')[p_\infty - p_R]\,d\gamma/dT = G\,\rho\,\rho'\,(s-s')\,\gamma_0 - \rho\,g\,(\rho-\rho')\,\gamma(T_\infty), \tag{49}$$

which can be used to search for oscillatory instabilities.

An example for the water-steam system with $T_R = 640$ K is shown in Fig. 8. Here we have taken $T_\infty = T_R$ and $p_\infty = 1.0681\,p_R$ in order to obtain an oscillatory neutral mode with $R = R_c = 0.1\mu$m, with a corresponding temperature gradient of $G = G_c = -21.713$ K/m, as determined from Eq. (49). In Fig. 8 we show the real part of the growth rate, σ_r, versus the radius of a steady state bubble. Each radius in the plot has an associated temperature gradient G that determines the size of the bubble under steady-state conditions. The stability of each bubble is indicated in the plot, with smaller bubbles being stable, and larger bubbles being unstable. The solid curves in the plot correspond to direct modes with $\sigma_i = 0$, and the dashed curves correspond to complex conjugate modes with $\sigma_i \neq 0$. The loss of stability occurs to an oscillatory mode where the curve crosses the axis $\sigma_r = 0$ with $R = R_c$ and $G = G_c$, where we find $\sigma_i = \pm 1.6873$ s^{-1}. Oscillatory modes also occur for the case $T_R = 373.15$ K, but require considerably

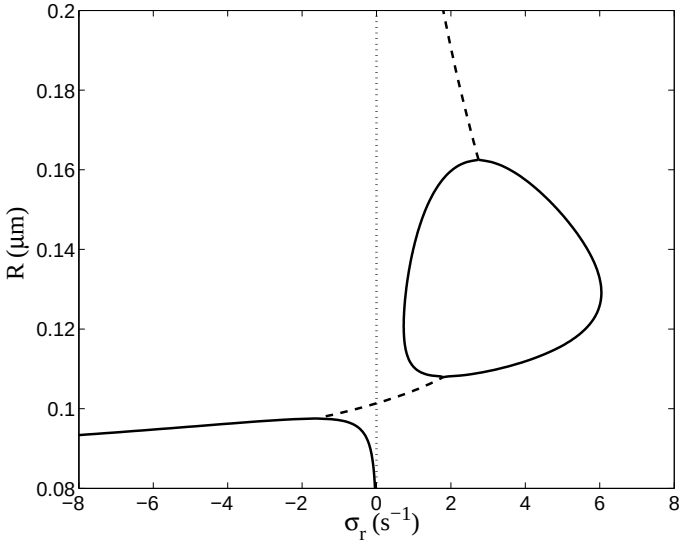

Figure 8: Linear stability of a steady-state bubble of steam in water with radius R, under the conditions $T_R = 640K$, $p_R = 2.027 \times 10^7$ Pa, $T_\infty = T_R$, and $p_\infty = 1.0681\, p_R$. The solid curves correspond to direct modes of instability with $\sigma_i = 0$, and the dashed curves correspond to complex conjugate pairs with $\sigma_i \neq 0$. The dotted line denotes the demarcation between stability and instability ($\sigma_r = 0$).

larger values of p_∞ that are likely to exceed the range of validity of our linearized equation of state (9).

3.5 Numerical Solution

A time-dependent numerical solution to the nonlinear equations (17) and (18) is shown in Fig. 9. The conditions correspond to those of Fig. 8, but with a temperature gradient of $G = -22.3714$ K/m. For this gradient the corresponding steady-state bubble with $R = 0.1015$ μm is linearly unstable with $\sigma = 0.0527 \pm i1.7119$ s^{-1}. The nonlinear solution (solid curve) shows oscillatory growth in time, leading to a predicted disappearance of the bubble at time $t = 31$ s. The linearized solution (dashed curve), normalized to have the same initial radius, $R(0) = 0.1065$ μm, shows good agreement for small times, both

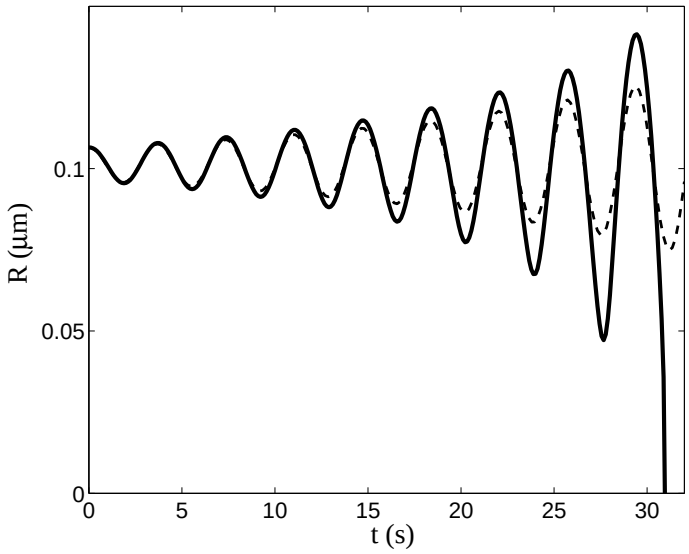

Figure 9: Oscillations of an unstable bubble of steam in water with $T_R = 640$ K. The solid curve shows a numerical solution of the nonlinear governing equations, and the dashed curve shows a comparison with the linearized solution. The nonlinear oscillations become large enough that the bubble disappears at finite time.

in amplitude and frequency of oscillation. Beyond $t = 31$ s the bubble radius given by the numerical solution becomes negative, and the nonlinear equations no longer provide an adequate description of the process.

3.6 Weakly-Nonlinear Solution

Near the critical conditions of Fig. 8 at $R = R_c = 0.1\mu$m and $G = G_c = -21.713$ K/m where the bubble loses stability to an oscillatory mode there are solutions that oscillate periodically in position and radius and satisfy the nonlinear governing equations. These solutions bifurcate from the point of marginal stability and may be described by a weakly-nonlinear theory that describes the amplitude and period of the solution in the vicinity of the bifurcation point. The solution is given by a formal expansion in a small parameter

δ,

$$R(\bar{t},\delta) = R_c + R^{(1)}(\bar{t})\delta + R^{(2)}(\bar{t})\delta^2 + R^{(3)}(\bar{t})\delta^3 + ... \tag{50}$$

with a similar expression for $Z(\bar{t},\delta)$. Here the expansion parameter δ is defined in terms of the deviation of G from the critical temperature gradient G_c,

$$G(\delta) = G_c + G_1\delta + G_2\delta^2 + ..., \tag{51}$$

and $\bar{t}$ is a rescaled time, $\bar{t} = \omega(\delta)t$, with

$$\omega(\delta) = \omega_0 + \omega_1\delta + \omega_2\delta^2 + ... \tag{52}$$

The leading order solution is given by the steady state solution at $G = G_c$, and the first order correction is described by linear stability theory, with, for example,

$$R^{(1)}(\bar{t}) = \mathcal{A}\cos\bar{t}. \tag{53}$$

The constant ω_0 is given by the critical value of σ_i at the onset of instability. We denote the maximum and minimum radius over a period of oscillation of the nonlinear solution by $R_{\max}$ and $R_{\min}$, so that for small amplitudes we have $R_{\max} \approx R_c + \delta\mathcal{A}$ and $R_{\min} \approx R_c - \delta\mathcal{A}$. The general goal of this type of weakly-nonlinear expansion is to determine the oscillation amplitude $R_{\max} - R_c \sim \delta\mathcal{A}$ and period $\tau(\delta) = 2\pi/\omega(\delta)$ of the oscillation as functions of $G(\delta) - G_c$; the parameter δ is introduced as a convenient parametrization for this dependence. This determination occurs by applying solvability conditions to the hierarchy of equations that result from a formal expansion in powers of δ. For this type of problem the symmetry of the problem with respect to sign changes of the type $\mathcal{A} \to -\mathcal{A}$ leads to an expansion with $\omega_1 = 0$ and $G_1 = 0$, and the solvability conditions then ensure that the third order equations contain no resonant inhomogeneities that would generate non-periodic ("secular") solutions. These conditions typically take the form of "amplitude equations" of the general form

$$\mathcal{A}\left(\mathcal{C}\mathcal{A}^2 - \omega_2\right) = 0, \tag{54}$$

$$\mathcal{A}\left(\mathcal{D}\mathcal{A}^2 - G_2\right) = 0, \tag{55}$$

where the coefficients $\mathcal{C}$ and $\mathcal{D}$ depend on the material constants (ρ^*, μ^*, etc.) and control parameters (T_∞, p_∞, etc.) For $\mathcal{D} \neq 0$ one sets $G_2 = \mathcal{D}/|\mathcal{D}| = \pm 1$, which effectively serves to define δ. Supercritical bifurcating solutions with $G > G_c$ (stable in time) are then obtained for $\mathcal{D} > 0$ and subcritical bifurcating solutions with $G < G_c$ (unstable in time) are obtained for $\mathcal{D} < 0$. The amplitude is then given by $\mathcal{A}^2 = 1/\mathcal{D}$, and the frequency correction is $\omega_2 = \mathcal{C}/\mathcal{D}$.

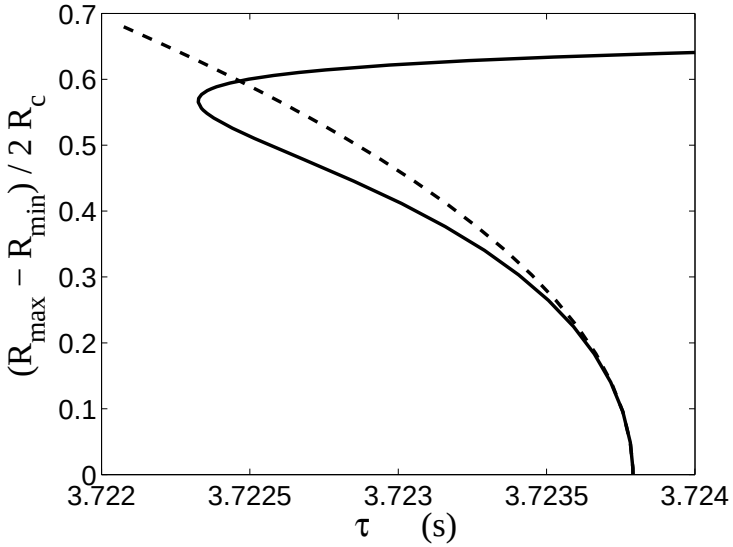

Figure 10: Comparison of weakly nonlinear theory (dashed curve) with the nonlinear solution (solid curve) for an oscillating bubble of steam in water with $T_R = 640$ K. The normalized amplitude $[R_{\max} - R_{\min}]/2R_c$ is shown as a function of the temporal period $\tau = 2\pi/\omega$.

In our particular case, however, we find that the solvability conditions gives $\mathcal{D} = 0$ and $\mathcal{C} \neq 0$, so that $G_2 = 0$ and the dependence of amplitude on $G - G_c$ must be determined by continuing to higher order in the expansion, which we have not pursued. At third order we are left with the relation $\mathcal{A}^2 = \omega_2/\mathcal{C}$, which we have compared with a numerical solution of the nonlinear equations in Fig. 10. For the same conditions of Fig. 8 the weakly nonlinear analysis gives the value $\mathcal{C}^{-1} = 0.001682$ s m^2, which produces the dashed parabolic curve in Fig. 10. Guided by the weakly nonlinear results, the nonlinear

numerical solution is obtained by a shooting method which produces a time-periodic solution with a given amplitude by varying the values of the gradient G and temporal period $\tau = 2\pi/\omega$. We find that the numerical solution (solid curve in Fig. 10) satisfies $G = G_c$ to eight digits over this range, with good agreement with the weakly nonlinear theory at small amplitudes. The period of the numerical solution initially decreases over a small range of values, then reaches a limit point and increases with increasing amplitude. In Fig. 11 we show the numerical solution at a large amplitude, with $R_{\max}/R_c = 1.414$ and $R_{\min}/R_c = 0.05$. The bubble nearly disappears during the course of the oscillation and the radius $R(t)$ shows significant nonlinear distortion; the solution for $Z(t)$ is nearly sinusoidal.

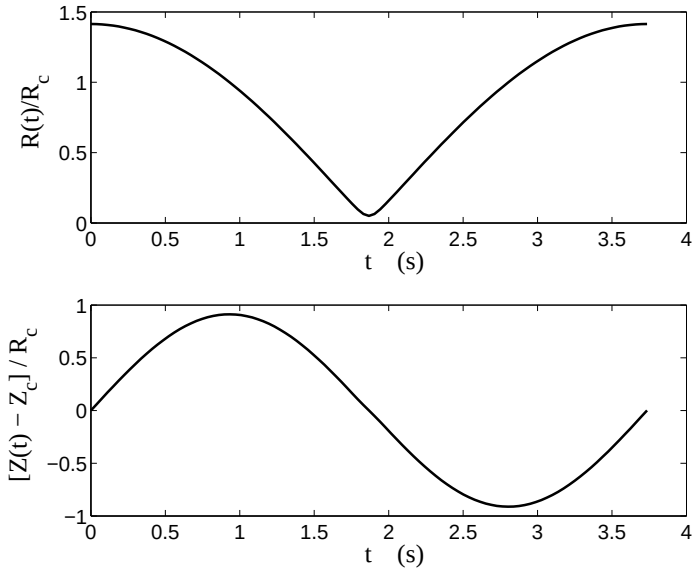

Figure 11: Oscillations of a bubble of steam in water with $T_R = 640$ K. The normalized bubble radius is $R(t)/R_c$, and the normalized bubble position is $(Z(t) - Z_c)/R_c$, where R_c and Z_c are the critical radius and position of the marginally-stable bubble with $\sigma_r = 0$

4 Discussion

The solutions we have computed correspond to conditions of small Reynolds number $\mathrm{Re} = RV/\nu$ and small Peclet number PrRe, where Pr is the Prandtl number. For the conditions of the water-steam system illustrated in Fig. 2 both Re and Pe are much less than one. The dimensionless oscillation frequency $\sigma_i R^2/\nu$ that we find is also much less than unity, consistent with the quasistatic governing equations (4) and (5). The spherical drop is an analytical solution in the small Reynolds number approximation. For immiscible drops, modifications of the shape of the spherical drop for larger values of Re are discussed by Subramanian and Balasubramaniam [1], who also include more general inertial effects on the immiscible solution. The solutions that we obtain correspond to drops that are undergoing a phase change accompanied by an incompressible flow; the resulting oscillations are not caused by compressibility effects. We have not considered non-spherical distortions of the surface, though these effects could be included in a more general linear stability analysis. We have followed Young, Goldstein, and Block in assuming that the material properties (other than surface energy) are independent of temperature; this approximation is probably valid for the range of temperature gradients that we have considered.

We have presented numerical calculations mostly for the case of heating from below ($G < 0$), although the governing equations (17) and (18) are valid for temperature gradients of either sign. For heating from below the Marangoni force on either a bubble or a drop is in the downward direction, and with an immiscible interface a stationary state ($\dot{Z} = 0$) can be obtained only for a bubble ($\rho' < \rho$) which experiences an upward buoyancy force. To obtain a stationary state for an immiscible drop ($\rho' > \rho$) one must heat from above ($G > 0$), so that buoyancy and Marangoni forces can again balance. For the case of a phase-changing drop or bubble, however, heating from below can result in either stationary drops or bubbles under the right conditions, since the phase-change effect, proportional to $[s - s']$, changes sign in tandem with $[\rho - \rho']$ if the phases are interchanged.

We have obtained solutions that oscillate in size and position for a single-component, phase-changing system. We note that a drop or bubble with an immiscible interface cannot undergo purely radial oscillations if the flow is incompressible, since there is no local mass flux through the interface. The observed oscillations in the model can therefore be attributed generally to the effects of phase change, which do allow mass flux through the interface. A more detailed explanation for the oscillations is complicated by the variety of the physical mechanisms considered in the model, including those of viscosity, buoyancy, thermocapillarity, and phase change. However, for the specific numerical example of a steam bubble ($\rho' < \rho$, $L < 0$) with heating from below ($G < 0$) shown in Fig. 8 we can extract the dominant mechanisms at play. The oscillatory state is obtained as an instability of a stationary bubble, so that the considerations include: i) conditions for the occurrence of the underlying steady state itself; ii) conditions for the neutral stability of a perturbation ($\sigma_r = 0$); and iii) conditions for the occurrence of an oscillatory response ($\sigma_i \neq 0$). Firstly, in the numerical example in Fig. 8, the steady state represents a balance between buoyancy and phase-change effects (c.f. Fig. 5 for $R = 0.1\mu$m); the Marangoni effect is unimportant. Secondly, in the condition (49) for neutral stability ($\sigma_r = 0$), the dominant balance is found to be between the thermocapillary term proportional to $d\gamma/dT$ and the phase-change term proportional to $[s - s']$; the buoyancy term proportional to $g(\rho - \rho')$ is unimportant. Thirdly, the conditions for oscillation ($\sigma_i \neq 0$) which require $\beta\epsilon < 0$ in Eq. (47) (with $\alpha = 0$) are found to hold with $\beta < 0$ and $\epsilon > 0$. More specifically, the dominant terms in β and ϵ under these conditions are found to be

$$\beta = \frac{-kG}{\rho' LR}, \quad \epsilon = \frac{4e_3}{d_2} g(\rho - \rho')R, \tag{56a,b}$$

which do lend themselves to a physical interpretation in terms of a balance between phase change and buoyancy effects. The disturbance equations (44) reduce to

$$\delta\dot{R} = \beta\delta Z, \quad \delta\dot{Z} = \epsilon\delta R \tag{57a,b}$$

under neutral conditions ($\sigma_r = 0$). With $\epsilon > 0$ Eq. (57b) expresses the tendency of a larger bubble ($\delta R > 0$) to rise ($\delta\dot{Z} > 0$) due to buoyancy, and vice versa. Eq. (56b) for ϵ

is related to the linearization of Eq. (23) for the Stokes velocity due to buoyancy. On the other hand with $\beta < 0$ Eq. (57a) states that if a bubble is displaced downward ($\delta Z < 0$), it tends to grow ($\delta \dot{R} > 0$) due to the phase change effect. That is, with $G < 0$, a bubble that is displaced downward encounters hotter fluid, and the gas phase grows at the expense of the liquid phase due to evaporation. Similarly, a bubble displaced upward to lower temperatures tends to shrink due to liquid condensation at the interface. Eq. (56a) for β is related to the linearization of Eq. (36) for the growth in bubble radius during thermal migration in a temperature gradient. The cycle of oscillation is therefore that a downward displacement produces an increase in bubble radius due to evaporation at higher temperatures; the larger bubble then rises due to increased buoyancy. Overshooting its original position, it then rise to regions of colder temperature, where it shrinks and falls due to reduced buoyancy to repeat the cycle.

Our expression (18) for the drop velocity contains terms proportional to the temperature gradient G and the gravitational acceleration g, just as in the analogous expression (22) obtained by Young et al. However, our expression contains a number of additional materials parameters, resulting in a more complicated dependence on the drop radius R. As a consequence a number of distinguished limits for the drop velocity are possible. For example, keeping the leading order terms in the G and g expressions gives, in the limit of small latent heat (or small R),

$$V = \frac{-e_1}{d_3} GR \frac{d\gamma}{dT} + \frac{e_5}{d_3}(\rho - \rho')gR^2 \tag{58}$$

for $d_3 \neq 0$ (see appendix for coefficients), expressing a balance between thermocapillary and buoyancy forces in determining V. On the other hand, in the limit of large latent heat (or large R)

$$V = \frac{-e_2}{d_2} \frac{G}{L} + \frac{e_3}{d_2}(\rho - \rho')gR^2, \tag{59}$$

expressing a balance between phase change effects and buoyancy forces in determining V, independent of thermocapillary effects. Surprisingly, in an idealized, density-matched system ($\rho' = \rho$), we have $d_3 = 0$ and $e_1/e_2 = d_1/d_2$, and so (for any value of L) Eq. (18)

reduces to the simple result for thermal migration (see Section 3.3),

$$V = \frac{-3\,k\,G}{\rho\,L}. \tag{60}$$

Since L changes sign under an interchange of the phases, this result is analogous to the experimental observations by Califano et al. [7] that α-phase particles and β-phase particles in a binary alloy can move in opposite directions in a given temperature gradient.

5 Conclusion

We have considered the motion of a drop or bubble in a vertical temperature gradient under the influence of buoyancy, thermocapillarity, and phase change effects. We consider drops or bubbles of one fluid phase in another fluid phase of the same single-component material, and treat the coupled effects of thermal diffusion and convection in each phase. The associated boundary conditions include the release of latent heat upon a change of phase at the surface, and also permit flow through the surface of the bubble, in contrast to the case of the thermal migration of an immiscible drop. An explicit solution for a spherical drop is found that results in a set of two coupled ordinary differential equations governing the rate of change of the drop radius and position. The steady state solutions of these equations generally describe a balance between buoyancy and thermal effects. For smaller drops the results are similar to those for the immiscible case treated by Young, Goldstein, and Block [3], while for larger drops the Marangoni effect can be overwhelmed by the effects of latent heat release; a similar dominance of Marangoni effects by phase-change effects can be obtained in a layer geometry [14, 15]. In particular, the limiting case of dominant phase change effects produces motion in the direction of $-G/L$ [see Eq. (37)], in contrast to the Marangoni effect in which the velocity is in the direction of $-Gd\gamma/dT$ [see Eq. (22)]. This is consistent with experimental observations of Califano et al. [7] for drop motion in a binary alloy. We have analyzed the linear stability of the steady-state solutions of the governing equations, and found conditions that lead to unstable modes corresponding to solutions that oscillate in position and ra-

dius. We have also performed a weakly-nonlinear analysis of the oscillatory modes, and compared with a numerical solution of the nonlinear equations. The occurrence of oscillatory behavior in this model is in qualitative agreement with experimental observations of drop oscillations in multicomponent systems for which the diffusion of solute plays a significant role. Special cases of the results include the description of growth during a phase transformation, stability of a critical nucleus, and liquid zone migration during material processing. Numerical results are given for material properties corresponding to a water-steam system near atmospheric pressure and near the critical point.

6 Acknowledgments

A.K.N is grateful for support from a NIST-ARRA Postdoctoral Fellowship administered by the University of Maryland College Park.

Table I

Thermophysical properties of the steam (α phase) water (β phase) system

Reference temperature	T_R	640	373.15	K
Reference pressure	p_R	$202.7(10^5)$	$1.01325(10^5)$	Pa
density of water	ρ_β	481.6	965.0	kg/m^3
density of steam	ρ_α	177.4	0.585	kg/m^3
dynamic viscosity of water	μ_β	$5.526(10^{-5})$	$2.8(10^{-4})$	Pa s
dynamic viscosity of steam	μ_α	$2.795(10^{-5})$	$1.25(10^{-5})$	Pa s
thermal conductivity of water	k_β	0.4177	0.68	W/mK
thermal conductivity of steam	k_α	0.2499	0.025	W/mK
surface energy	γ	$8.09(10^{-4})$	$5.89(10^{-2})$	J/m^2
$d\gamma/dT$	γ_T	$-1.42(10^{-4})$	$-1.95(10^{-4})$	J/K m^2
difference in entropy density	$s_{\alpha\beta} = s_m^\alpha - s_m^\beta$	$8.632(10^2)$	$6.049(10^3)$	J/K kg
difference in enthalpy density (latent heat)	$L_{\alpha\beta} = h_m^\alpha - h_m^\beta$	$5.524(10^5)$	$2.257(10^6)$	J/kg
gravitational acceleration	g	9.8	9.8	m/s^2

7 Appendix

The material constants that appear in Eqs. (17) and (18) are given by

$$e_1 = 90k\mu\mu^*[2+\rho^*] \tag{A1}$$

$$e_2 = 27k\mu\rho\rho^*(2\rho^* + \mu^*[2+\rho^*]) \tag{A2}$$

$$e_3 = 6\rho^2(1+\mu^*)(\rho^*)^2 \tag{A3}$$

$$e_4 = 2\rho\rho^*(10\mu^* - \rho^*) \tag{A4}$$

$$e_5 = 3\mu k(2+k^*)[2(\rho^*)^2 + 20\mu^* - 8\mu^*\rho^* + \mu^*(\rho^*)^2] \tag{A5}$$

$$d_1 = 90\mu\rho\mu^*\rho^* \tag{A6}$$

$$d_2 = 9\mu\rho^2(\rho^*)^2(2+3\mu^*), \tag{A7}$$

$$d_3 = 180k\mu^2\mu^*(2+k^*)(1-\rho^*), \tag{A8}$$

where $\rho^* = \rho'/\rho$, $\mu^* = \mu'/\mu$, and $k^* = k'/k$.

In Eqs. (13) through (16) the velocity components, pressure and temperature fields for both inside and outside of the drop have been expressed in terms of unknowns that are determined by applying the boundary conditions at the bubble interface. Two of these unknowns $\dot{R}$ and $\dot{Z}$ are stated in Eqs. (17) and (18). The remainder of the unknowns have been expressed in terms of $\dot{R}$ and $\dot{Z}$ and are given below

$$a = \frac{1}{3}\rho g\, R^3(1-\rho^*), \tag{A9}$$

$$F = T_\infty + G\, Z + \frac{LR\rho\rho^*}{k}\dot{R}, \tag{A10}$$

$$b_0 = R^2(1-\rho^*)\dot{R}, \tag{A11}$$

$$B = \frac{LR^2\rho\rho^*}{k}\dot{R}, \tag{A12}$$

$$a_0 = \rho\,\rho^*\,(s-s')(T_R-T_\infty-G\,Z)+\big(p_R(1-\rho^*)+\rho^*\,p_\infty\big)-\frac{1}{k}\Big(LR(s-s')\rho^2\,(\rho^*)^2\dot{R}\Big). \quad \text{(A13)}$$

The rest can be compactly expressed as rational functions with a common denominator, D given by

$$D = \mu\Big(60k\mu\mu^*(2+k^*)+3\rho^2(\rho^*)^2(s-s')(2+\mu^*)LR^2+10LR\rho\,\mu^*\rho^*(d\gamma/dT)\Big). \quad \text{(A14)}$$

The numerators also share common properties in that they can be expressed in the form $[x_i]G+[x_j]V+[x_k](1-\rho^*)\rho g$, so that

$$B' = \frac{[180k\mu^2\mu^*]G+[60L\mu^2\,\rho\mu^*\,\rho^*]V+LR^2[\mu\rho^2\rho^*\Big(2\rho^*+\mu^*(10+\rho^*)\Big)](1-\rho^*)g}{\rho D}, \quad \text{(A15)}$$

$$A = R^3\,(B'-G), \quad \text{(A16)}$$

$$a' = \frac{[x_1]G+[x_2]V+[x_3](1-\rho^*)\rho g}{3\rho D}, \quad \text{(A17)}$$

where x_1, x_2 and x_3 are given by

$$x_1 = -540k(s-s')\mu^2\,\rho^2\,\mu^*\rho^* \quad \text{(A18)}$$

$$x_2 = -180L\mu^2\,\rho^3\,\mu^*(\rho^*)^2\,(s-s') \quad \text{(A19)}$$

$$x_3 = 10\mu\,\rho\mu^*\rho^*\big(3LR^2(s-s')\rho^2\rho^*+LR\rho\rho^*\,(d\gamma/dT)+6\mu\,k(2+k^*)\big), \quad \text{(A20)}$$

$$b' = \frac{[x_4]G+[x_5]V+[x_6](1-\rho^*)\rho g}{6\rho D} \quad \text{(A21)}$$

where x_4, x_5 and x_6 are given by

$$x_4 = 9k\rho R\big(3R\mu\,\rho\rho^*(s-s')(4+\mu^*)+10\mu\mu^*\,(d\gamma/dT)\big) \quad \text{(A22)}$$

$$x_5 = 18\mu\rho\big(LR^2(s-s')\rho^2(\rho^*)^2 - 10k\mu\mu^*(2+k^*)\big) \tag{A23}$$

$$x_6 = -R^2\Big(3LR^2(s-s')\rho^3(\rho^*)^2 + 3k\mu\rho(2+k^*)(\mu^*(-10+\rho^*)+4\rho^*) + LR\rho^2(\rho^*)^2(d\gamma/dT)\Big), \tag{A24}$$

$$c = \frac{[x_7]G + [x_8]V + [x_9](1-\rho^*)\rho g}{6\mu\rho D} \tag{A25}$$

where x_7, x_8 and x_9 are given by

$$x_7 = -18kR^4\rho\mu^2\mu^*\left(3R\rho\rho^*(s-s') + 10(d\gamma/dT)\right) \tag{A26}$$

$$x_8 = -6LR^4\mu^2\rho^2\mu^*\rho^*\big(3R\rho\rho^*(s-s') + 10(d\gamma/dT)\big) \tag{A27}$$

$$x_9 = R^5\mu\rho\rho^*\Big(6k\mu\mu^*(2+k^*) + 3LR^2\rho^2\,\mu^*\,\rho^*(s-s') + 2LR\mu\rho(5\mu^* - \rho^*)(d\gamma/dT)\Big). \tag{A28}$$

References

[1] R. Shankar Subramanian and R. Balisubramaniam. *The Motion of Bubbles and Drops in Reduced Gravity*. Cambridge University Press, New York, 2001.

[2] S.H. Davis. Thermocapillary instabilities. *Ann. Rev. Fluid Mech.*, 19:403–435, 1987.

[3] N.G. Young, J. S. Goldstein, and M. J. Block. The motion of bubbles in a vertical temperature gradient. *J. Fluid Mech.*, 6:350–356, 1959.

[4] S.C. Hardy. The motion of bubbles in a vertical temperature gradient. *Journal of Colloid and Interface Science*, 69:157–162, 1979.

[5] R.H. Merritt and R.S. Subramanian. The migration of isolated gas bubbles in a vertical temperature gradient. *J. Colloid Interface Sci.*, 125:333–339, 1988.

[6] F. Morick and D. Woermann. Migration of air bubbles in silicone oil under the action of buoyancy and thermocapillarity. *Ber. Bunsenges. Phys. Chem.*, 97:961–969, 1993.

[7] Filomena Califano, Roberto Mauri, and Reuel Shinnar. Large-scale, unidirectional convection during phase separation of a density-matched liquid mixture. *Physics of Fluids*, 17:094109, 2005.

[8] B. Mutaftschiev. Nucleation theory. In D.T.J. Hurle, editor, *Handbook of Crystal Growth, Vol. 1A*, pages 189–247. North-Holland, Amsterdam, 1993.

[9] S.H. Davis. *Theory of Solidification*. Cambridge University Press, New York, 2001.

[10] W.W. Mullins and R.F. Sekerka. Morphological stability of a particle growing by diffusion or heat flow. *J. Appl. Phys.*, 34:323–329, 1963.

[11] W.A. Tiller. Migration of a liquid zone through a solid: Part i. *Journal of Applied Physics*, 34:2757–2762, 1963.

[12] T.R. Anthony and H.E. Cline. The Stability of Migrating Droplets in Solids. *Acta Metallurgica*, 21:117–122, 1973.

[13] G.K. Batchelor. *An Introduction to Fluid Mechanics*. Cambridge University Press, New York, 1970.

[14] G.B. McFadden, S.R. Coriell, K.F. Gurski, and D.L. Cotrell. Onset of convection in two liquid layers with phase change. *Physics of Fluids*, 19: 104109, 2007.

[15] G.B. McFadden,, S.R. Coriell, and P.A. Lott. Onset of convection in two layers of a binary liquid. *J. Fluid Mech.*, 647: 105-124, 2010.